

Study of the isoscalar scalar $bc\bar{u}\bar{d}$ tetraquark T_{bc} with lattice QCD

Archana Radhakrishnan^{1,*}, M. Padmanath^{2,3,†} and Nilmani Mathur^{1,‡}

¹*Department of Theoretical Physics, Tata Institute of Fundamental Research,
Homi Bhabha Road, Mumbai 400005, India*

²*The Institute of Mathematical Sciences, CIT Campus, Chennai, 600113, India*

³*Homi Bhabha National Institute, Training School Complex, Anushaktinagar, Mumbai 400094, India*



(Received 19 April 2024; accepted 17 June 2024; published 6 August 2024)

We present a lattice QCD study of the elastic S -wave $D\bar{B}$ scattering in search of tetraquark candidates with explicitly exotic flavor content $bc\bar{u}\bar{d}$ in the isospin $I = 0$ and $J^P = 0^+$ channel. We use four lattice QCD ensembles with dynamical u/d , s , and c quark fields generated by the MILC collaboration. A nonrelativistic QCD Hamiltonian, including improvement coefficients up to $\mathcal{O}(\alpha_s v^4)$, is utilized for the bottom quarks. For the rest of the valence quarks we employ a relativistic overlap action. Five different valence quark masses are utilized to study the light quark mass dependence of the $D\bar{B}$ scattering amplitude. The finite volume energy spectra are extracted following a variational approach. The elastic $D\bar{B}$ scattering amplitudes are extracted employing Lüscher's prescription. The light quark mass dependence of the continuum extrapolated amplitudes suggests an attractive interaction between the \bar{B} and D mesons. At the physical pseudoscalar meson mass ($M_{ps} = M_\pi$) the $D\bar{B}$ scattering amplitude has a subthreshold pole corresponding to a binding energy of $-39(^{+4}_{-6})(^{+8}_{-18})$ MeV with respect to the $D\bar{B}$ threshold. The critical M_{ps} at which the $D\bar{B}$ scattering length diverges and the system becomes unbound corresponds to $M_{ps}^* = 2.94(15)(5)$ GeV. This result can hold significant experimental relevance in the search for a bound scalar T_{bc} tetraquark, which could well be the next “doubly heavy” bound tetraquark to be discovered with only weak decay modes.

DOI: [10.1103/PhysRevD.110.034506](https://doi.org/10.1103/PhysRevD.110.034506)

I. INTRODUCTION

The study of exotic hadrons is one of the most prominent areas of research in contemporary particle physics. The proliferating list of discovered exotic hadrons, exhibiting properties that demand interpretations beyond conventional meson and/or baryon models, continues to captivate the scientific interest. A compilation of various exotic hadrons discovered till now and their properties can be found in Ref. [1]. Among these exotic hadrons, those with manifestly exotic flavor content having four quarks in their valence structures are particularly popular. Several of them are proximal to open flavor thresholds pointing to a connection with the corresponding scattering channel for their existence, and possibly their nature. These four quark states could be compact tetraquarks, or meson-meson

molecular excitations, or a mixture of both or something more intriguing: a much enviable research topic at this time. An in-depth understanding of the binding mechanism governing these hadrons can play a crucial role in elucidating the nonperturbative QCD dynamics.

A particularly notable common feature among the discovered four quark hadrons is the presence of at least one heavy quark constituent in their valence structure. Phenomenologically it has been hypothesized and discussed that a color-singlet combination of two very heavy quarks (antiquarks) and two light antiquarks (quarks) can form a $QQ\bar{q}_1\bar{q}_2$ bound state [2,3]. Recently a handful of calculations using first principles method of lattice QCD also strongly indicate the presence of deeply bound states with the quark contents $bb\bar{q}_1\bar{q}_2$; $q_1 \in u, d$; $q_2 \in d(s), u(s)$ [4–9]. Very interestingly a doubly charmed four quark hadron, coined as T_{cc}^{++} , with the quark content $cc\bar{u}_1\bar{d}_2$ and unusually long lifetime, has recently been discovered by LHCb [10]. Lattice QCD calculations have also investigated T_{cc}^{++} and suggested that the existence of this hadron could be the result of a delicate fine tuning between the light and heavy quark masses [11–14]. In summary, lattice QCD calculations and phenomenological investigations consistently suggest the existence of deeply bound states

*Contact author: archana.radhakrishnan@tifr.res.in

†Contact author: padmanath@imsc.res.in

‡Contact author: nilmani@theory.tifr.res.in

Published by the American Physical Society under the terms of the [Creative Commons Attribution 4.0 International license](https://creativecommons.org/licenses/by/4.0/). Further distribution of this work must maintain attribution to the author(s) and the published article's title, journal citation, and DOI. Funded by SCOAP³.

in doubly bottom four quark system, referred to as $T_{bb} \in bb\bar{q}_1\bar{q}_2$, while experimental evidence has been reported for a four quark hadron (T_{cc}) with the quark content $cc\bar{u}\bar{d}$. Notably, the charm quark mass is comparatively lighter than the bottom quark mass, suggesting potentially differing binding strengths for doubly bottomed and doubly charmed four quark states due to QCD dynamics operating at multiple scales.

In this respect, four quark systems ($T_{bc} \in bc\bar{q}_1\bar{q}_2$), which are in between T_{bb} and T_{cc} , i.e., with a bottom and a charm valence quarks, are of particular interest. Phenomenologically, predictions on the existence of such states are ambiguous with their energies exhibiting considerable spread over several hundreds of MeV around the relevant two-meson threshold. Several model studies based on heavy quark symmetry [15–17] suggest no binding. Numerous nonchiral models [18–29] also suggest either a weak binding or an unbound system. However, certain chiral models [30–33] and QCD sum rule investigations [34–38] propose a more pronounced binding. Some recent studies like [39] also predict a bound state.

In such a scenario, first principles lattice QCD calculations can provide much needed information on the bindings of T_{bc} states. However, previous lattice QCD calculations [40–42] claim either no evidence for a bound T_{bc} state or insufficient statistics to conclude its existence. In Ref. [42], the authors do not come up to a conclusion due to large uncertainties. In a recent work, we investigated the $J^P = 1^+$ channel considering chiral as well as continuum extrapolations and found an attractive interaction between the \bar{B}^* and D mesons indicating the possible existence of a bound T_{bc} state with a binding energy of $-43^{(+6)}_{(-7)}{}^{(+14)}_{(-24)}$ MeV with respect to the $D\bar{B}^*$ threshold [43]. Afterwards, in another recent calculation [44], some of the authors of Ref. [42] studied $J^P = 0^+$ as well as 1^+ channels, involving bilocal two-meson interpolators corresponding to the elastic excitations of $D\bar{B}^{(*)}$ scattering. They found attractive interactions in both channels, and subsequently pointed to the existence of shallow bound states. Given the coarse lattices they utilize for these hadrons with two heavy quarks, it will be important to check whether the binding of these states observed in Ref. [44] will survive or enhance with continuum extrapolation.

Motivated by the recent progress, and building upon our previous work for $J^P = 1^+$ channel [43], in this work we perform a lattice QCD calculation of elastic $D\bar{B}$ mesons¹ scattering in the isoscalar scalar channel $I(J^P) = 0(0^+)$. Following a partially quenched approach, we investigate the light quark mass dependence of the $D\bar{B}$ mesons scattering. The lattice-extracted scattering amplitudes,

¹We assume $m_u = m_d$, ignore QED effects, and refer to the degenerate (D^+B^- , $D^0\bar{B}^0$) threshold as $D\bar{B}$.

employing Lüscher’s finite-volume prescription, are extrapolated to the continuum limit. The amplitude at the physical pion mass is deduced following a study of the light quark mass dependence of these continuum-extrapolated results. Finally, the hadronic pole information in this physical amplitude is studied towards identification of bound state poles.

Experimentally, $J^P = 0^+$ channel is also more interesting as it could be the next “doubly heavy” tetraquark to discover since it has a reduced heavy diquark mass that is lower than that for the $bb\bar{q}_1\bar{q}_2$ system. It would also likely be the first tetraquark that would unambiguously decay only weakly.

The remainder of the manuscript is structured as follows. A brief overview of our lattice setup is provided in Sec. II. In Sec. III, we discuss various relevant technical details involved in our calculation such as the observable measured, the interpolating operators utilized and the extraction of finite volume energy spectra, which are presented in Sec. IV. The extraction of scattering amplitudes, continuum extrapolations, and chiral extrapolations made are presented in Sec. V. In Sec. VI we present a discussion on the bindings of T_{bc} four-quark states, in perspectives of available lattice and nonlattice results, along with a comparison of scattering lengths for DD^* , $D\bar{B}^*$, BB^* , and $D\bar{B}$ scatterings. Finally we summarized our results in Sec. VII.

II. LATTICE DETAILS

The computational setup used in this calculation is similar to the one in several of our previous publications [7,45–54] and most recently in Ref. [43]. We use four $N_f = 2 + 1 + 1$ ensembles with dynamical quark fields respecting a highly improved staggered quark (HISQ) action generated by the MILC collaboration [55]. Other relevant details of various lattice QCD ensembles used are listed in Table I. The lattices have different volumes and lattice spacings a , which are estimated using the r_1 parameter [55]. The gauge fields respect one-loop and follow the tadpole-improved Symanzik gauge action with tuned coefficients through $\mathcal{O}(\alpha_s a^2, n_f \alpha_s a^2)$ [56]. The valence quark masses up to the charm quark are realized using an overlap fermion action that is $\mathcal{O}(am)$ improved [57,58]. The bare charm quark mass on each ensemble was tuned using the kinetic mass of spin averaged $1S$ charmonia $\{a\bar{M}_{\text{kin}}^{cc} = 0.75aM_{\text{kin}}(J/\psi) + 0.25aM_{\text{kin}}(\eta_c)\}$ determined for the respective ensembles following the Fermilab prescription [59] (for more details see Refs. [48,49]). The bare strange quark mass is tuned to the physical point such that the lattice estimate for the fictitious pseudoscalar $\bar{s}s$ equals 688.5 MeV [60].

Our setup assumes an exact isospin symmetry $m_u = m_d$ over a range of light quark masses corresponding to $M_{ps} \sim 0.5, 0.6, 0.7$ (equivalent to the strange quark mass), 1.0, and 3.0 (equivalent to the charm quark mass) GeV, to

TABLE I. Details of lattice QCD ensembles employed. M_{ps}^{sea} refers to the sea pion mass. S_1 , S_2 , and S_3 refer to small spatial volume ensembles and L_1 refers to the large volume ensemble.

Ensemble	Symbol (a) [fm]	Lattice spacing ($N_s^3 \times N_t$)	Dimensions	M_{ps}^{sea}
S_1	\diamond	0.1207(11)	$24^3 \times 64$	305
S_2	\blacklozenge	0.0888(8)	$32^3 \times 96$	312
S_3	\circ	0.0582(4)	$48^3 \times 144$	319
L_1	\square	0.1189(9)	$40^3 \times 64$	217

map the light quark mass dependence over a wide range of M_{ps} values. In Fig. 1, we present the landscape of different light quark masses (in terms of M_{ps}) studied in the lattice ensembles employed. We utilize a wall-smearing procedure at the quark source for our propagator measurements which is described in Refs. [7,51,54].

We use a nonrelativistic QCD (NRQCD) Hamiltonian approach for the bottom quark [61]. The bottom quark mass was tuned following the Fermilab prescription [59], matching the lattice-determined kinetic mass of the spin-averaged $1S$ bottomonium state to its experimental value. For details regarding the NRQCD Hamiltonian, improvement coefficients, and bottom quark mass tuning specific to our setup, see Ref. [50].

III. DETERMINING THE FINITE VOLUME SPECTRA USING LATTICE QCD

The time dependence of Euclidean two-point correlation functions

$$C_{ij}(t) = \sum_{\mathbf{x}} \langle \mathcal{O}_i(\mathbf{x}, t) \tilde{\mathcal{O}}_j^\dagger(0) \rangle = \sum_n \frac{Z_i^n Z_j^{n\dagger}}{2E^n} e^{-E^n t}, \quad (1)$$

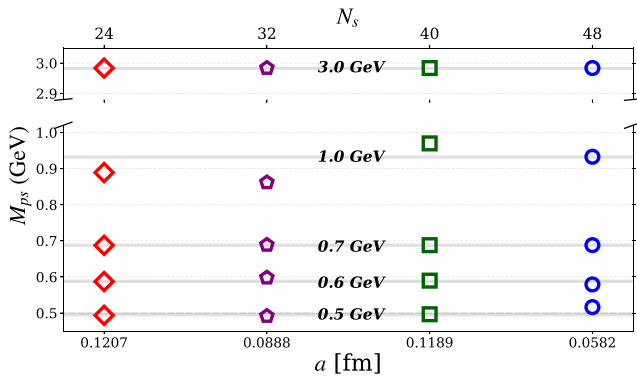


FIG. 1. A landscape plot of the pseudoscalar masses used across the different lattice ensembles. The light quark masses are varied across these five values, while charm and bottom quarks are tuned to their physical values. The horizontal gray bands represent estimates of M_{ps} , to facilitate a comparison of pseudoscalar meson masses across all four ensembles.

featuring operators $\mathcal{O}_i(\mathbf{x}, t)$ with the desired quantum numbers dictate the time evolution of finite volume spectral levels. Here the operator-state overlap $Z_i^n = \langle 0 | \mathcal{O}_i | n \rangle$ determines the coupling of the operator \mathcal{O}_i with the state n . The wall-smearing at the quark source in our setup filters out all the high-momentum modes at the source, whereas at the sink time slice we utilize a point sink for the quark fields and project the correlation function to its rest frame as shown in Eq. (1). This asymmetric nature of the wall-source point-sink setup is emphasized in Eq. (1) with different operators and the operator-state overlaps at the source and at the sink.

For the \bar{B} and D mesons, we compute two-point correlation functions using the standard local quark bilinear interpolators $(\bar{Q} \Gamma q)$ with spin structure $\Gamma \sim \gamma_5$. Since we are only interested in the rest frame ground state, single meson correlation functions are evaluated only for the A_1^- irrep in the finite volume.

Our study focuses on the S -wave $D\bar{B}$ scattering in the rest frame leading to infinite volume quantum numbers $J^P = 0^+$, which reduces to the A_1^+ finite-volume irrep. The elastic two-meson threshold is at $E_{D\bar{B}} = m_D + m_{\bar{B}}$, whereas the lowest inelastic threshold corresponds to the $D^* \bar{B}^*$ scattering channel, which is sufficiently high to assume a purely elastic $D\bar{B}$ scattering in the S -wave. There are no relevant low lying three particle thresholds in this channel and the lowest multiparticle inelastic threshold corresponds to $D\bar{B}\pi\pi$.

In the present analysis, we use both a meson-meson type of operator and a local diquark-antidiquark kind of operator as in Ref. [41]:

$$\begin{aligned} \mathcal{O}_1(x) &= [\bar{u}(x)\gamma_5 b(x)][\bar{d}(x)\gamma_5 c(x)] \\ &\quad - [\bar{d}(x)\gamma_5 b(x)][\bar{u}(x)\gamma_5 c(x)], \\ \mathcal{O}_2(x) &= (\bar{u}(x)^T \Gamma_5 \bar{d}(x)) \\ &\quad - \bar{d}(x)^T \Gamma_5 \bar{u}(x)(b(x)\Gamma_5 c(x)). \end{aligned} \quad (2)$$

Here $\mathcal{O}_1(x)$ is a meson-meson operator associated with the $D\bar{B}$ threshold with the individual D and \bar{B} forming a color singlet. We do not include any other scattering operators since the next one, corresponding to the $D^* \bar{B}^*$ is sufficiently higher up in energy and is assumed to have negligible effects on the low-lying spectrum. Excited elastic two-meson operators of $D\bar{B}$ system with nonzero relative meson momenta, such as those used in Ref. [44], are also not utilized in this study. The wall-smearing setup we utilize disallows construction of such elastic scattering operators.

$\mathcal{O}_2(x)$ is a local diquark-antidiquark type operator where all the (anti)quark fields are jointly projected to zero momentum. In the color space, diquarks/antidiquarks are built in the antitriplet/triplet representations of $SU(3)_c$. In Eq. (2), $\Gamma_k = C\gamma_k$ with $C = i\gamma_2\gamma_4$ being the charge conjugation matrix. Phenomenologically, doubly heavy

tetraquarks are expected to be deeply bound and compact in the heavy quark limit, which motivates the use of this operator [5,62]. Such compact local operators were also considered in our previous study [43] of axial-vector bottom-charm tetraquarks. It is also empirically known from several other studies of doubly bottom tetraquarks that such operators have a rich overlap with the ground state [41,42,63–68].

With these two operators, we find a suitable linear combination that overlaps maximally to the ground state by solving for the generalized eigenvalue problem [69],

$$\mathcal{C}(t)v^n(t) = \lambda^n(t)\mathcal{C}(t_0)v^n(t). \quad (3)$$

The eigenvalues, $\lambda^n(t)$ correspond to the n^{th} lowest eigenstates with energy E^n , where $n \leq 1$ in our case. We are only interested in the ground state E^0 . The time evolution of the lowest eigenvalue, $\lim_{t \rightarrow \infty} \lambda^0(t) \sim A_0 e^{-E^0 t}$, gives the value of the ground state energy in the large time limit, whereas the magnitude of the operator state overlaps

$$Z_i^0 = \langle 0 | \mathcal{O}_i | 0 \rangle = \sqrt{2E^0} (V^{-1})_i^0 e^{E^0(t_0)/2}, \quad (4)$$

indicates the coupling of the operators to the ground state. Here V is the matrix of eigensolutions $v^n(t)$, which are expected to be time independent in the large time limit, where $\mathcal{C}(t)$ is saturated by the lowest N eigenstates.

The quality of signals in the energy estimates are assessed using the effective energies,

$$aE_{\text{eff}} = [\ln(\mathcal{C}(t)/\mathcal{C}(t + \delta t))]/\delta t, \quad (5)$$

cf. Fig. 2, where we plot present aE_{eff} for the case $M_{ps} \sim 3$ GeV on the finest lattice. The black points represent the

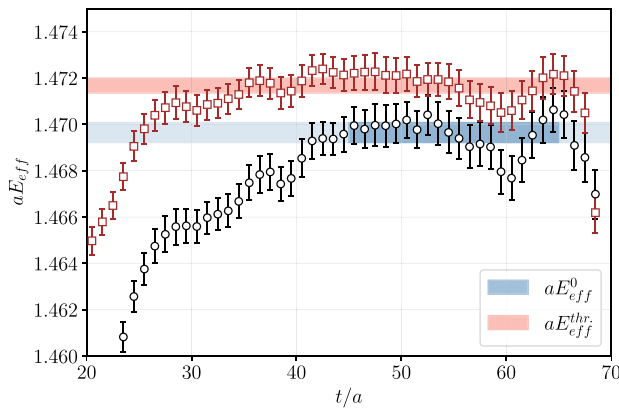


FIG. 2. Effective energy plot for the eigenvalue of the ground state $\lambda^0(t)$ in circular black markers and for the lowest threshold which is the product of single-meson correlators for the D and \bar{B} meson, $\mathcal{C}_D(t)\mathcal{C}_{\bar{B}}(t)$ in square red markers. The corresponding blue and orange bands are the energy fit estimates using single exponential fit forms on $\lambda^0(t)$ and the single-meson correlation functions, respectively.

effective energy of the interacting system $\mathcal{C}(t) = \lambda^0(t)$, whereas the red points indicate the effective energy of the correlator $\mathcal{C}(t) = \mathcal{C}_D(t)\mathcal{C}_{\bar{B}}(t)$ of the noninteracting system of D and \bar{B} mesons and serve as a reference. A negative shift of the interacting energy level with respect to the noninteracting ones is evident in Fig. 2.

The energy estimates are extracted from the correlator data from fitting them with their expected asymptotic forms. This can be performed in two ways: the obvious way of fitting the interacting correlator $\lambda^0(t)$ directly or to fit the ratio of correlators

$$R^0(t) = \frac{\lambda^0(t)}{\mathcal{C}_D(t)\mathcal{C}_{\bar{B}}(t)}, \quad (6)$$

with a single exponential form in the large time limit. We are primarily interested in determining the energy splittings between the interacting data and the noninteracting one, $\Delta E^0 = E^0 - M_D - M_{\bar{B}}$. Fits to $R^0(t)$ directly leads to the estimates for ΔE^0 . Alternatively, these splittings can be evaluated as differences between the estimates for energy E^0 from fits to $\lambda^0(t)$ and for $(M_D, M_{\bar{B}})$ from separate fits to $\mathcal{C}_D(t)$ and $\mathcal{C}_{\bar{B}}(t)$, respectively. A comparison of estimates from these two procedures assures that the ground state energy splittings we extract are not influenced by any conspired cancellation of noises leading to any fake energy plateaus. We present a demonstration of such a comparison in Fig. 3, where it is evident that the value of ΔE^0 estimated from the two different procedures agree with each other within error bars. This trend is observed throughout all the correlators examined. The final results quoted in this paper are based on fitting the ratio correlators defined in Eq. (6).

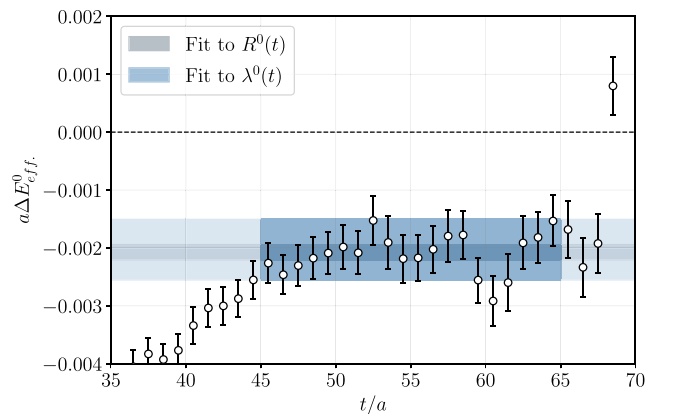


FIG. 3. $a\Delta E^0$ versus t/a plot, for $M_{ps} \sim 3$ GeV on the finest lattice. Here $a\Delta E^0(t)$, shown in the circular black data datapoints, is the effective energy splitting determined using Eq. (5) with $\mathcal{C}(t) = R^0(t)$. The fit estimates determined from the single exponential fits to $\lambda^0(t)$ and $R^0(t)$ is shown in gray and blue bands, respectively.

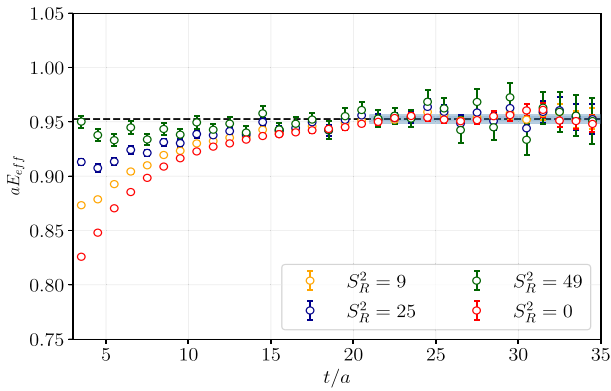


FIG. 4. A comparison of effective energies for the ground state between the asymmetric wall-source point-sink setup ($S_R^2 = 0$, red points) and those extracted with various box smearing radius-squared $S_R^2 = 9, 25, 49$ in the wall-source box-sink setup [41]. The smearing radius squared are presented in units of the lattice spacing. The black dashed line is the fit estimate for the ground state energy with $S_R^2 = 0$, with blue horizontal band showing the fitting window and error bar.

As emphasized in the preceding text, the wall-source point-sink setup can efficiently suppress the nonzero momentum excitations providing a cleaner access to the ground state energy. However, a drawback of this setup is that the different smearings at the source and sink can result in coefficients in the spectral decomposition of the two-point functions that are not positive definite. This renders the matrix of two-point correlation functions to be asymmetric. Hence, it is possible that the effective energies could approach their asymptotic values as rising from below, as opposed to a conventional expected monotonic falling-from-above behavior. This is evident from the red points in Fig. 4 showing the behavior of aE_{eff} from wall source and point sink setup. If the fitting window is not sufficiently distant from the source, there could be misleading low-lying plateaus at early times that mimic the actual ground state plateau. This can result in incorrect estimates of the energy difference between the true ground state and the threshold.

The comparison of the energy splitting obtained from the nonratio correlators [Eq. (5)] and the ratio correlators [Eq. (6)] in Fig. 3, helps in validating the robustness of the ground state. Additionally, to investigate any remnant associated systematic effect of the above-mentioned pattern (rising from below) of effective energies, we also use a setup with wall-smear source and box-smear sink with various radii (S_R). This exercise helps to study the asymptotic approach to the symmetric limit, where the effective energies are expected to display a falling-from-above behavior as the box smearing radius (S_R) increases [41]. We have employed such setup previously in Refs. [43,54] to demonstrate the asymptotic behavior in axial-vector T_{bc} tetraquarks, and fully bottomed dibryons.

In Fig. 4, we plot the time dependence of the ground state effective energies, for the case where the pseudoscalar mass $M_{ps} \sim 0.7$ GeV on the finest lattice we use. The datapoints in different colors represent different smearing radius-squared of the box-sink $S_R^2 = 9, 25, 49$, in units of lattice spacing. The data with $S_R^2 = 0$ represents the results with point-sink setup. We clearly observe that, as the smearing radius increases, the effective mass approaches the symmetric limit with the falling-from-above feature, but is noisier compared to the wall-source point-sink setup ($S_R^2 = 0$). With the blue shaded region and dashed black line we also show the fitting-window and fitted-value of the ground state with its error bar, obtained from the wall-source setup. The presence of consistent effective mass plateaus for all the values of the smearing radius assure that the value of the ground states extracted from the asymmetric setup does not deviate from the symmetric setup at large enough times.

IV. FINITE VOLUME SPECTRA

In Fig. 5, we present the extracted finite-volume energy spectra of the $0(0^+)$ $bc\bar{u}\bar{d}$ channel on the four ensembles listed in Table I, at the five different $m_{u/d}$ values corresponding to roughly, $M_{ps} \sim 0.5, 0.6, 0.7, 1.0, \text{ and } 3.0$ GeV. The energy spectrum shown is normalized by the threshold $M_D + M_{\bar{B}}$, such that center-of-mass energy at threshold is unity in these units. In each panel, the x axis represents the spatial extension of the lattice.

The finite-volume energies are determined from energy splittings extracted from the ratio correlators given in Eq. (6). These energy splittings are free of the additive offsets, inherent to the NRQCD formulation, as the numerator and denominator in Eq. (6) carries same number of valence NRQCD-based bottom quarks. The reconstruction of the finite-volume energies from the energy splittings follow the same lines as in Ref. [43].

A clear trend of negative shifts for the ground state energies with respect to the $D\bar{B}$ threshold can be observed for all the lattices and for all the quark masses studied. It is also evident that this negative shifts decreases in magnitude with increasing M_{ps} , as expected for a doubly heavy tetraquark system [5,62]. The variation in this splitting across different lattice spacings for any given M_{ps} is not transparent due to large uncertainties, whereas unlike in our study of axial-vector T_{bc} tetraquark, a moderate trend of decreasing splitting with increasing volume can be observed as expected. However, it is too early to substantiate this behavior considering the large uncertainties. Despite the large uncertainties, the consistent negative shifts clearly point to an attractive interaction between the D and \bar{B} meson in the scalar channel.

In the wall-smearing setup we use, the elastic $D\bar{B}$ excitations involving nonzero relative meson momenta are suppressed. This should not affect the ground state

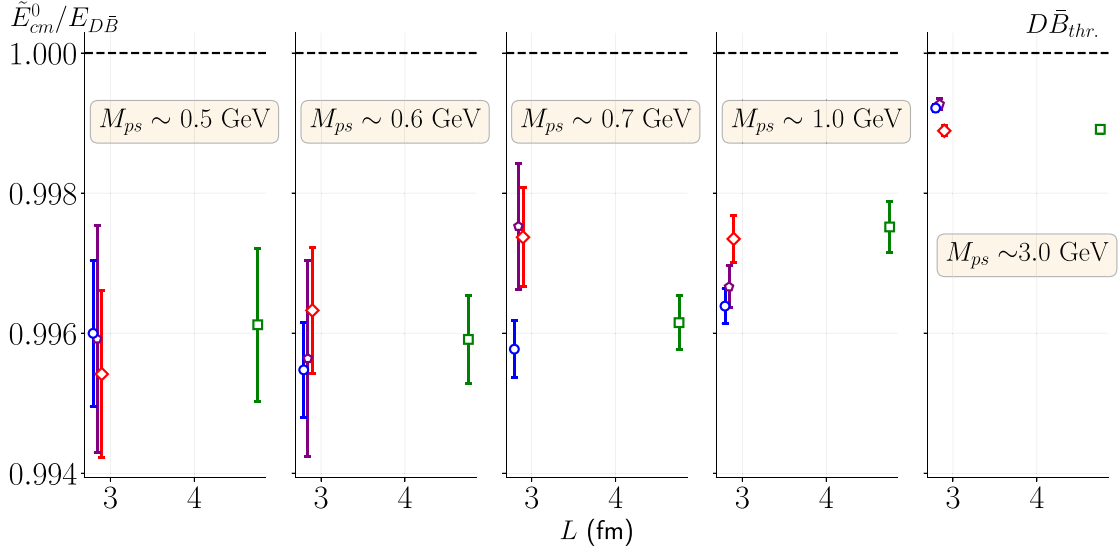


FIG. 5. The ground state finite volume energies in the $0(0^+) bc\bar{u} \bar{d}$ channel. Different panels stand for different M_{ps} values indicated on the top of the respective channel. The y axis indicates the energy in the center-of-mass frame, in units of energy of the $D\bar{B}$ threshold. The x axis in each panel indicates the spatial extent of the lattice ensembles used.

determination because it is unlikely that operators with relative momenta contribute to the ground state. Additionally, we employ various cross checks that helps us estimate the excited state contaminations in the ground state energy, that are then included in the systematic uncertainties. We refrain from using or plotting the excited states determined from the solutions of Eq. (3) in Fig. 5, as they do not represent the elastic $D\bar{B}$ excitations in the wall-smearing setup. Another significant limitation of the wall-smearing setup is its asymmetry, leading to the possibility of the ground-state energy plateau being approached from below. The agreement observed between the energy splittings calculated from ratios of correlators and those determined from the difference in energy fit estimates for individual single meson and interacting two-meson correlators indicates that our correlator-based fitting estimates effectively manage contaminations from excited states which are then incorporated into the systematic errors.

V. $D\bar{B}$ SCATTERING AMPLITUDE FROM THE FINITE-VOLUME SPECTRA

In this section, we present S -wave elastic $D\bar{B}$ scattering amplitudes determined following Lüscher's finite-volume prescription [70]. We use only the ground state energies to constrain the amplitudes, since the wall-smearing procedure that we utilize for quark sources is not suited to extract the elastic excitations but only the ground states [43]. For the scalar channel considered in this work, the lowest inelastic threshold is $D^*\bar{B}^*$, which is significantly high in energy and there are no higher partial wave that can mix with the S -wave, justifying an elastic S -wave analysis.

A topical aspect in the study of doubly heavy hadrons is the influence of left-hand cuts due to off-shell pion exchanges [71]. Recently, there has been efforts to accommodate the left-hand cut effects arising from single pion exchanges [72–74]. In $D\bar{B}$ scattering, the closest non-analyticity below the threshold can happen from an off-shell two-pion exchange, which has its branch point well below the elastic threshold. Hence we ignore any effects of such left-hand nonanalyticities in our analysis.

A. Amplitude fits using Lüscher's finite-volume formalism

The Lüscher's finite-volume formalism relates the amplitude of two-particle scattering to the finite volume-spectrum in a cubic box. Particularly for the elastic S -wave scattering of B and D mesons,

$$k \cot[\delta_0(k^2)] = \frac{2Z_{00}[1; (\frac{kL}{2\pi})^2]}{L\sqrt{\pi}}, \quad (7)$$

where Z_{00} is the generalized zeta function described in Ref. [70], L is the spatial extent of the cubic box and $\delta_0(k)$ is the S -wave phase shift as a function of k , which is the momentum of either mesons in the center of momentum frame related to the center of momentum energy $E_{cm} = \sqrt{s}$ through $4s k^2 = (s - (M_D + M_{\bar{B}})^2)(s - (M_D - M_{\bar{B}})^2)$. From Eq. (7), it is clear that there is a one-to-one correspondence between the energy level and the $\delta_0(k)$, i.e., each finite-volume energy level provides a specific value of the S -wave elastic phase shift with which one can constrain the energy or k dependence of the phase shift.

We perform the amplitude fits with the ground states from all four ensembles listed in Table I, and repeat this for all five values of M_{ps} indicated in Fig. 1. The fits follow minimization of a cost function defined as

$$\chi^2 = \sum_{i,j} (f(k_i^2) - f(\{A\}, k_i^2)) \times (\mathcal{C}^{-1})_{ij} (f(k_j^2) - f(\{A\}, k_j^2)), \quad (8)$$

where $f(k_i^2)$ is the amplitude [lhs of Eq. (7)] extracted from the simulations at k_i^2 , and $f(\{A\}, k_i^2)$ is the parametrization of the energy dependence of the amplitude. \mathcal{C} is the covariance matrix defined as in Ref. [75]. We verify that the results determined from the χ^2 defined in Eq. (8) are consistent with that one gets from the procedure outlined in Appendix B of Ref. [14]. Considering the smallness of $(k/E_{D\bar{B}})^2$ and the limited energy range over which the ground states are placed, we assume a zero-range approach for the amplitude parametrization. Additionally, we include a linear lattice spacing dependence to account for the cutoff effects in the extracted amplitude, which takes the form

$$k \cot[\delta_0] = A^{[0]} + aA^{[1]}, \quad (9)$$

where $A^{[0]} = -1/a_0$, with a_0 being the scattering length in the continuum limit.

In Figs. 6 and 7, we present the fit results to $k \cot[\delta_0]$ (the bands) as a function of the lattice spacing and $(k/E_{D\bar{B}})^2$, respectively, along with the lattice data. The bands in Fig. 7 are the continuum extrapolated results given by the parameter $A^{[0]}$. Different horizontal panels represent different M_{ps} values. The best fit parameters and corresponding quality of fits are tabulated in Table II.

Given the negative energy shifts and the sign of $A^{[0]} = -1/a_0$, determines the nature of the near-threshold poles, if any. Note that for the noncharm light quark masses, a_0 is consistently positive suggesting that the strength of interaction to be sufficient enough to house a bound state. Whereas at the charm point a_0 is negative, despite negative energy shifts, suggesting only a feeble interaction that cannot hold a subthreshold pole with square-integrable wave function. This is similar to our observation in the axial-vector channel using the same setup and formalism in Ref. [43], as well as to the phenomenological expectation for doubly heavy four quark systems, here the binding energy is expected to decrease with increasing light quark masses for fixed heavy quark masses.

Another interesting observation is on the variation in the cut off dependence of the amplitudes as the light quark masses are varied. The cutoff dependence is accounted by the parameter $A^{[1]}$, which shows a signature change as the light quark mass increases towards the charm point. This suggests that for a doubly heavy four quark ($QQ'l_1l_2$) system with $(m_{l_1} = m_{l_2}, m_Q, m_{Q'} \gg m_l)$, the cut off effects weaken the finite-volume energy splitting of the ground

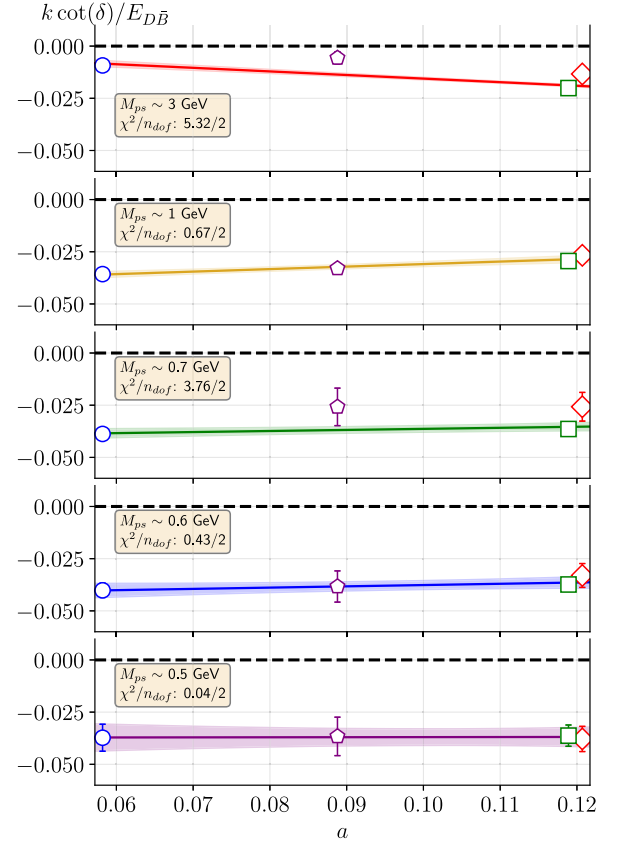


FIG. 6. $k \cot[\delta_0]$ normalized by the elastic threshold $E_{D\bar{B}}$, versus lattice spacing, a , for the M_{ps} values studied in this analysis as indicated in the different panels. The colored bands indicate the fit results to the amplitude parametrization given in Eq. (9). The marker conventions are as listed in Table I. For all the M_{ps} values except when $M_{ps} \sim 3.0$ GeV, the fits show a positive scattering length a_0 , indicating an attractive interaction.

state with the elastic threshold. On the other hand, close to the charm point (where $m_Q, m_{Q'} \sim m_l$) such effects enhance this energy splitting in the $QQ'l_1l_2$ system determined in a finite volume. Relatively large errors at the noncharm M_{ps} values partially obscure these effects, if any exist, while at the charm point such effects are clearly reflected. Any further quantified comments on this lattice spacing dependence is currently beyond the scope of the current work, particularly considering the large uncertainties.

B. Extrapolation to physical light quark mass

Following the extraction of the continuum extrapolated amplitude at different M_{ps} values, we delve into the light quark mass dependence of the fitted parameters. The leading order M_{ps} term in the chiral expansion suggests the M_{ps} dependence of hadron masses for light $m_{u/d}$ values ($m_q \lesssim \Lambda_{\text{QCD}}$) to be M_{ps}^2 . Whereas in the heavy light quark mass regime ($m_q \gg \Lambda_{\text{QCD}}$) heavy hadron masses are expected to be linear in M_{ps} [76]. With these phenomenological expectations, we use three fit forms like [43]

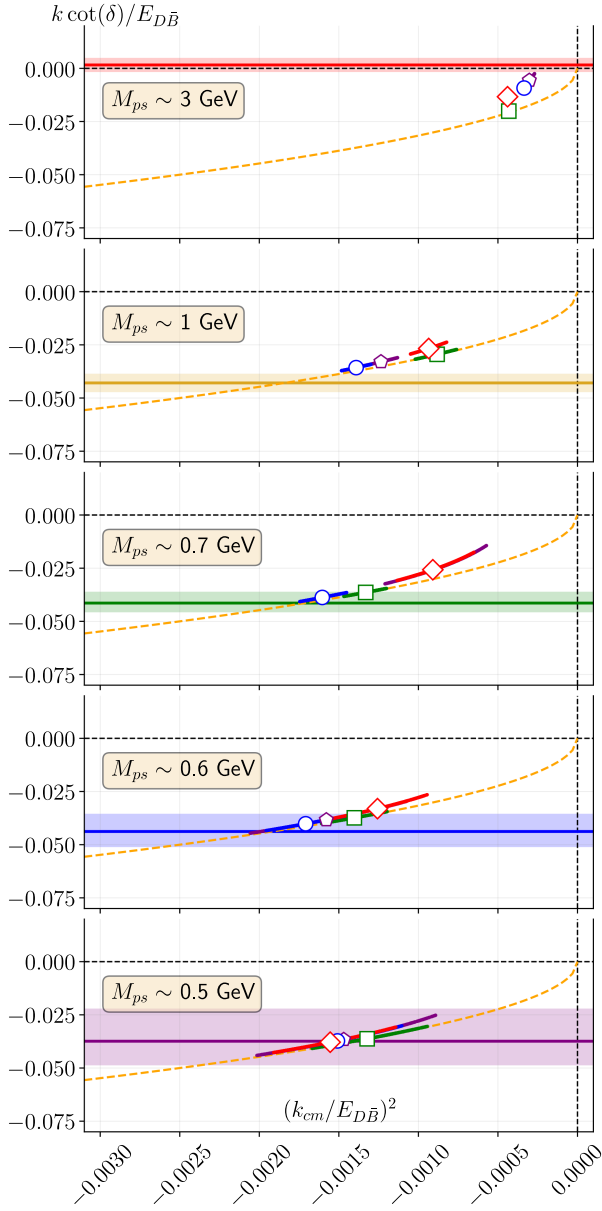


FIG. 7. $k \cot[\delta_0]$ versus k^2 for the different M_{ps} values shown in the legend. The scales in either axis are plotted in units of elastic $D\bar{B}$ threshold $E_{D\bar{B}}$. The dashed orange curve is the unitarity parabola related to the existence of a real bound state pole in the scattering amplitude. The horizontal bands are the continuum extrapolated amplitudes in Eq. (7) for each M_{ps} , also listed in Table II.

$$\begin{aligned}
 f_l(M_{ps}) &= \alpha_c + \alpha_l M_{ps}, \\
 f_s(M_{ps}) &= \beta_c + \beta_s M_{ps}^2, \quad \text{and} \\
 f_q(M_{ps}) &= \theta_c + \theta_l M_{ps} + \theta_s M_{ps}^2.
 \end{aligned} \quad (10)$$

The light quark mass dependence is determined by minimizing another cost function. The function is defined in terms of the differences in the data with the phenomenologically

TABLE II. Fit results for amplitude with parametrization given in Eq. (9) at various light quark masses, corresponding to M_{ps} in the first column. The optimized parameter values in the table are expressed in units of the energy of the threshold, $E_{D\bar{B}}$. The numbers within the parenthesis indicate the statistical errors.

M_{ps} [GeV]	$\chi^2/\text{d.o.f}$	$A^{[0]}/E_{D\bar{B}}$	$A^{[1]}/E_{D\bar{B}}$
0.5	0.04/2	$-0.038^{(+15)}_{(-11)}$	$0.004^{(+122)}_{(-134)}$
0.6	0.43/2	$-0.044^{(+8)}_{(-7)}$	$0.06(7)$
0.7	3.76/2	$-0.042^{(+5)}_{(-4)}$	$0.05^{(+5)}_{(-4)}$
1.0	0.67/2	$-0.043(4)$	$0.12(4)$
3.0	5.32/2	$0.002(3)$	$-0.17^{(+2)}_{(-3)}$

motivated parametrizations [cf. Eq. (10)] for its M_{ps} dependence and the data covariance. We present the results for this quark mass dependence in Fig. 8 together with the lattice extracted amplitudes as a function of $M_{ps}^2/E_{D\bar{B}}^2$. The two black symbols represents amplitude at the physical pion mass limit (y axis intercept; $M_{ps} = M_\pi$) and the critical mass (x axis intercept; M_{ps}^*) at which the system is close to unitarity branch point. The inner errors associated with these black symbols represent the statistical errors, whereas the outer errors also include systematic uncertainties added in quadrature.

The scattering length at the physical pion mass $M_{ps} = M_\pi$

$$a_0^{\text{phys}} = 0.61^{(+3)}_{(-4)}(18) \text{ fm} \quad (11)$$

together with the observed negative energy shifts in the interacting lattice levels indicate an attractive interaction between the B and D mesons, similar to the observation in Ref. [43]. This attraction is sufficiently strong enough to hold a real bound state with a binding energy

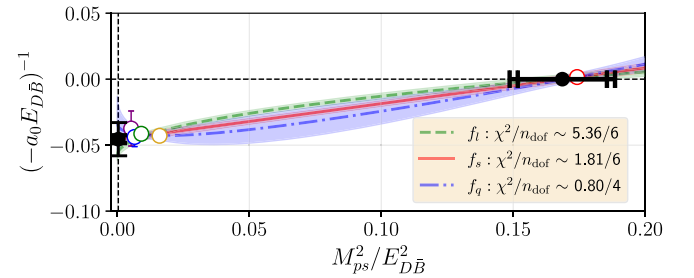


FIG. 8. The elastic $D\bar{B}$ scattering amplitude in the S -wave as a function of the light quark mass, in terms of the pseudoscalar mass squared M_{ps}^2 . The amplitude and M_{ps}^2 are presented in units of the energy of $D\bar{B}$ threshold ($E_{D\bar{B}}$). The bands indicate fits with different functional dependencies listed in Eq. (10). The vertical dotted line near the y axis represents the physical pion mass and the black star on it indicates the scattering amplitude in the physical limit. Another star symbol on the x axis indicates the critical M_{ps} where the $D\bar{B}$ system becomes unbound.

$$\delta E_{T_{bc}} = E_{T_{bc}} - E_{D\bar{B}} = -39_{(-6)}^{(+4)}_{(-18)}^{(+8)} \text{ MeV}. \quad (12)$$

When $m_{u/d} \gg \Lambda_{\text{QCD}}$, the leading linear behavior in M_{ps} is expected to be a good description. The black star at the x -axis intercept based on the linear M_{ps} dependence in Fig. 8 indicates the critical point

$$M_{ps}^* = 2.94(15)(5) \text{ GeV}, \quad (13)$$

at which a_0 changes its sign from negative to positive. M_{ps}^* and the associated errors are evaluated from the fit form $f_l(M_{ps})$ inspired by the leading linear behavior based on heavy quark effective field theory [76]. Note that the inverse scattering length at the charm point is consistent with zero and any fit form is constrained by the data at the charm point. Hence systematics associated with the critical mass estimates are significantly small compare to the statistical errors.

C. Systematic uncertainties

In this section we discuss various sources of uncertainties in this calculation that are summarized in Table III. We follow the bootstrap procedure to carefully carry the statistical errors. The most dominant systematics are observed to be associated with the light quark mass dependence in the chiral regime. Different chiral extrapolation fit forms lead to different estimates for the physical scattering length more significant than the statistical precision. The combination of $N_f = 2 + 1 + 1$ MILC lattice QCD ensembles we employ, together with the partially quenched setup using an overlap fermion action for light and charm quarks, and an NRQCD formulation for bottom quarks, and a rigorous heavy quark mass tuning procedure has been demonstrated to be quite efficient in extracting the ground states from finite volume. This setup also reproduces the $1S$ hyperfine splittings in quarkonia very precisely with uncertainties less than 6 MeV [50,54].

TABLE III. The error budget in the calculation of the scattering length, a_0^{phys} . This includes the systematics involved as a result of scale setting, excited state effects, heavy quark mass tuning, and uncertainties related to chiral and continuum extrapolations. The total systematics is determined by adding differential estimates in quadrature.

Source	Error [fm] $\times 10^2$
Statistical errors	$\begin{pmatrix} +3 \\ -4 \end{pmatrix}$
Scale setting	3
$m_{b/c}$ tuning	3
Excited states	4
Continuum extrapolation	8
Chiral extrapolation	15
Total systematics	18

The energy splittings and mass ratios we have adopted to work with, efficiently mitigate the systematics associated with the lattice realization of heavy quark dynamics [51,54]. We have also included the errors due to fit-window which includes the excited-state contamination. The values within the second parenthesis in Eqs. (11), (12), and (13) represent the cumulative systematic uncertainties added in quadrature where the uncertainties arising from chiral extrapolation fit forms can be observed to be dominant from Table III [51,54].

VI. DISCUSSION ON THE BINDINGS OF T_{bc}

At this stage, it is natural to assess, where our results stand among other existing lattice QCD-based and phenomenological calculations of $D\bar{B}(D\bar{B}^*)$ scattering in the isoscalar channels. Our investigations presented in this work (Ref. [43]) indicate negative finite-volume energy shifts in S-wave elastic scattering in $D\bar{B}(D\bar{B}^*)$ meson systems. Further analysis of scattering amplitude using finite volume Lüscher method points to the existence of a real square integrable bound state with binding energy of approximately 40 MeV in scalar [see Eq. (12)] and axial vector channels in Ref. [43]. While the error bar is large in the estimation in the binding energy, the conclusion on the attractiveness is robust. Recently another lattice QCD calculation with a different lattice setup has also confirms the attractive nature of interactions in both the channels, however, with a much lower binding, just below the respective threshold energies [43].

In Fig. 9, we present the results from various calculations on the binding of T_{bc} that have been predicted over the years. The results presented include those determined using lattice QCD and the nonlattice methods, separated by a horizontal line. In each plot, the vertical dashed lines are the respective elastic thresholds ($D\bar{B}$ for 0^+ and $D\bar{B}^*$ for 1^+). Results to the left of this vertical line suggests a bound state, whereas those lying to the right points to an unbound system. The vertical green bands are the results from our calculations (left: this work, right is from Ref. [43]) in perspective to those of other calculations. The left plot shows the results for $0(0^+)$ channel while the right one is for those of $0(1^+)$ channel. Estimates from nonlattice approaches seem to have a large spread of the order of several hundred MeV across the threshold. Both the lattice QCD results point towards the existence of bound states of T_{bc} . However, more detailed lattice calculations are necessary to find the exact locations and the nature of the bound state poles. Given these predictions from lattice QCD calculations, and considering the importance of the T_{bc} states as discussed in the introduction, experimental searches for these states would indeed be highly worthwhile in the near future.

Another interesting quantity to compare is the scattering length determining the small momentum meson-meson interactions in different doubly heavy quark systems (T_{bb} , T_{bc} , and T_{cc}) across various LQCD calculations. On the left

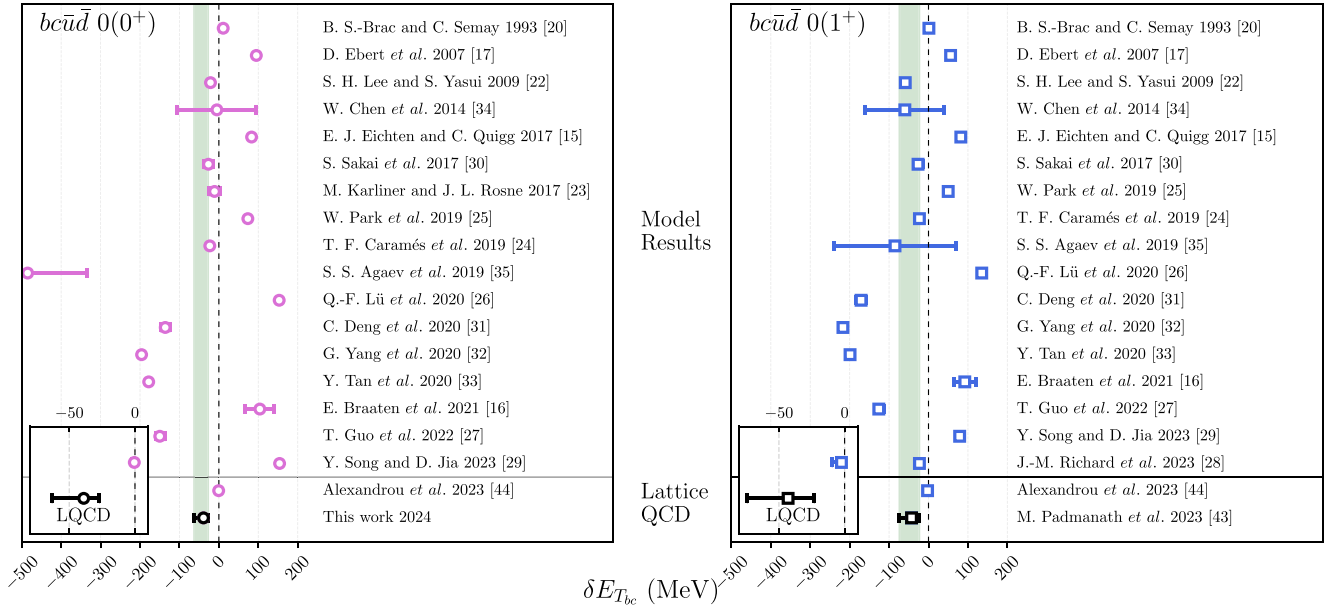


FIG. 9. The binding energy calculated in this work in comparison to the recent lattice QCD calculation [44] and other nonlattice determinations. Estimates from nonlattice approaches seem to have a mixed conclusion where several of them show shallow/deep binding and many others predicting an unbound state.

hand side of Fig. 10, we present the inverse scattering length ($1/a_0$) at the physical M_{ps} determined for these three exotic systems from different lattice calculations [8,12,43,77], where the [43] is our previous study using the same setup as the present study, together with the scattering length for the discovered T_{cc} [10]. The only other LQCD study of $D\bar{B}$ scattering [44] has also been included (faded point) for completeness albeit the analysis not being extrapolated to physical pion mass and to the continuum limit. The subscripts (H) and (L) in the x axis tick labels refer to two distinct procedures, the HALQCD and Lüscher-type finite-volume prescription followed, respectively, in extracting the scattering length. The HALQCD procedure followed in Refs. [12,77] provides quite precise estimates, whereas the large uncertainty in the

BB^* scattering using Lüscher-type procedure obscures extracting a possible trend, if any exist. Subduing these uncertainties require more finite-volume energy levels to constrain the amplitudes, which can be achieved either by extracting higher excited states, or by studying more ensembles at different volumes or at nonzero lab frame momenta [78]. In short, more followup studies involving rigorous Lüscher-type finite-volume treatments with precise estimates are highly desirable to make concrete procedure-independent statements on the bindings in different doubly heavy systems. A similar comparison of the scattering length in the S-wave scalar $D\bar{B}$ channel is shown on the right panel of Fig. 10. Considering the differences in systematics between the two evaluations (this work and Ref. [44]) for the $D\bar{B}^{(*)}$ systems, it is too early to argue on

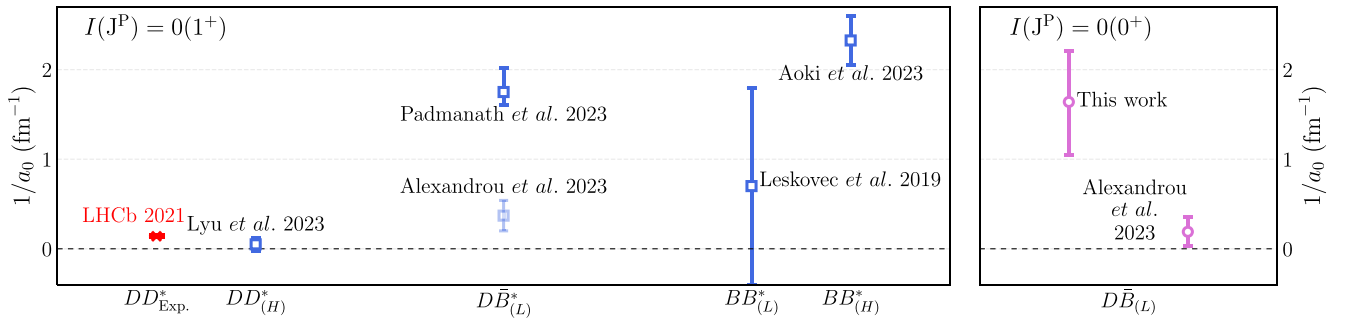


FIG. 10. Left plot: the inverse scattering length for DD^* , $D\bar{B}^*$, and BB^* scatterings at the physical pion mass as determined in Refs. [8,12,43,77]. The faded point corresponds to a recent lattice evaluation at an unphysically heavy pion mass [44]. Right plot: The inverse scattering length ($1/a_0$) in $D\bar{B}$ scattering compared between this work and Ref. [44].

the reasons for the observed discrepancies in the magnitude of scattering length and binding energy. It could possibly be related to the fact that the results from Ref. [44] lacks any chiral or continuum extrapolations or related to the lack of access to the excited elastic excitations in our work, which needs to be investigated further. Despite this discrepancy in the magnitude of scattering length, either calculations support attractive interactions in these systems. The large errors from our current study naturally indicate equally large uncertainty in the binding energy; however the fact that a bound state is seen is expected to be robust and consistent given the statistical relevance. Here again, more followup studies with a large number of interpolating operators and large statistics with rigorous Lüscher finite-volume analysis is highly desirable to obtain precise results.

VII. SUMMARY

In this work, we present a lattice QCD simulation of elastic S -wave $D\bar{B}$ scattering with explicitly exotic flavor $bc\bar{u}\bar{d}$ in the isoscalar scalar quantum numbers [$I(J^P) = 0(0^+)$]. We use four $N_f = 2 + 1 + 1$ ensembles with dynamical HISQ action generated by the MILC collaboration, with the valence quarks, up to the charm quark mass, realized using an overlap fermion action. The valence bottom quarks are described using an improved NRQCD formulation.

Using the ground state energy levels, presented in Fig. 5, we perform a rigorous finite-volume amplitude analysis using Lüscher's prescription. The analysis accounts for the lattice spacing effects by parametrizing the amplitude with a lattice spacing dependence, and taking the continuum limit separately for the five light quark masses studied. The quark mass dependence is then investigated to determine the elastic $D\bar{B}$ scattering length a_0^{phys} at the physical pion mass and the critical pseudoscalar mass M_{ps}^* at which a_0 diverges. The negative energy shifts in the ground state finite-volume energies taken together with the positive estimates for a_0^{phys} [presented in Eq. (11)] suggests an attractive interaction between the D and \bar{B} mesons that is strong enough to form a real square integrable bound state with binding energy of $-39_{(-6)}^{(+4)}_{(-18)}^{(+8)}$ MeV.

Recently another lattice QCD calculation on the $D\bar{B}$ systems also supports an attractive interaction between the mesons, however, with a smaller binding and closer to the threshold [44]. Note that this calculation employed bilocal two-meson-type operators at the source and sink and in extracting the relevant elastic excitations in the $D\bar{B}$

channel. However, the investigation is limited to two lattice ensembles with approximately similar lattice spacings (~ 0.12 fm), that is comparable to our coarsest lattice. The apparent discrepancy in the binding energy, whether it is a result of uncontrolled excited state contamination due to an asymmetric setup or if it is a result of uncontrolled discretization effects, remains to be understood. We leave this issue for the future lattice investigations.

In this study we are limited to rest frame ground states. While we are able to extract the amplitude with a zero-range approximation, future investigations with more rigor in extracting elastic excitations are necessary to constrain the energy dependence of the amplitude over a wider energy range. This would require meson-meson operators with zero overall momentum but individual momentum projected mesons like in Ref. [44] to extract the elastic excitations as well as meson-meson operators with nonzero overall momentum. Inclusion of such operators is beyond the scope of our current setup. Additionally, future studies involving fully dynamical simulations on a wider range of ensembles with different fermion actions, high-statistics studies with lighter up and down quark masses, and other improvements. These additional efforts would help constrain the relevant scattering amplitude in a framework-independent manner. In that journey, our calculation is an important step ahead where we have clearly shown the presence of an attractive interaction within the $D\bar{B}$ system, with controlled cutoff uncertainties and finite volume effects. Our findings offer a stride towards understanding the existence of $0(0^+)T_{bc}$, which could well be the next doubly heavy bound tetraquark to be discovered in the near future.

ACKNOWLEDGMENTS

This work is supported by the Department of Atomic Energy, Government of India, under Project Identification Number RTI 4002. M. P. gratefully acknowledges support from the Department of Science and Technology, India, SERB Start-up Research Grant No. SRG/2023/001235. We are thankful to the MILC collaboration and in particular to S. Gottlieb for providing us with the HISQ lattice ensembles. We thank the authors of Ref. [79] for making the *TwoHadronsInBox* package utilized in this work. Computations were carried out on the Cray-XC30 of ILGTI, TIFR. N. M. would also like to thank A. Salve and K. Ghadiali for computational support. M. P. would also like to thank Navdeep Singh Dhindsa for discussions.

- [1] Exotic hub, <https://qwg.ph.nat.tum.de/exoticshub/>.
- [2] R. J. Jaffe, Multiquark hadrons. i. phenomenology of $Q^2\bar{q}^2$ mesons, *Phys. Rev. D* **15**, 267 (1977).
- [3] R. L. Jaffe, $Q^2\bar{q}^2$ resonances in the baryon-antibaryon system, *Phys. Rev. D* **17**, 1444 (1978).
- [4] P. Bicudo, K. Cichy, A. Peters, and M. Wagner, BB interactions with static bottom quarks from lattice QCD, *Phys. Rev. D* **93**, 034501 (2016).
- [5] A. Francis, R. J. Hudspith, R. Lewis, and K. Maltman, Lattice prediction for deeply bound doubly heavy tetraquarks, *Phys. Rev. Lett.* **118**, 142001 (2017).
- [6] P. Bicudo, M. Cardoso, A. Peters, M. Pflaumer, and M. Wagner, $ud\bar{b}\bar{b}$ tetraquark resonances with lattice QCD potentials and the Born-Oppenheimer approximation, *Phys. Rev. D* **96**, 054510 (2017).
- [7] P. Junnarkar, N. Mathur, and M. Padmanath, Study of doubly heavy tetraquarks in lattice QCD, *Phys. Rev. D* **99**, 034507 (2019).
- [8] L. Leskovec, S. Meinel, M. Pflaumer, and M. Wagner, Lattice QCD investigation of a doubly-bottom $\bar{b}\bar{b}ud$ tetraquark with quantum numbers $I(J^P) = 0(1^+)$, *Phys. Rev. D* **100**, 014503 (2019).
- [9] R. J. Hudspith and D. Mohler, Exotic tetraquark states with two b^- quarks and $JP = 0+$ and $1+$ Bs states in a non-perturbatively tuned lattice NRQCD setup, *Phys. Rev. D* **107**, 114510 (2023).
- [10] R. Aaij *et al.* (LHCb Collaboration), Observation of an exotic narrow doubly charmed tetraquark, *Nat. Phys.* **18**, 751 (2022).
- [11] S. Collins, A. Nefediev, M. Padmanath, and S. Prelovsek, Towards the quark mass dependence of T_{cc}^+ from lattice QCD, *Phys. Rev. D* **109**, 094509 (2024).
- [12] Y. Lyu, S. Aoki, T. Doi, T. Hatsuda, Y. Ikeda, and J. Meng, Doubly charmed tetraquark T_{cc}^+ from lattice QCD near physical point, *Phys. Rev. Lett.* **131**, 161901 (2023).
- [13] S. Chen, C. Shi, Y. Chen, M. Gong, Z. Liu, W. Sun, and R. Zhang, $T_{cc}^+(3875)$ relevant DD^* scattering from $N_f = 2$ lattice QCD, *Phys. Lett. B* **833**, 137391 (2022).
- [14] M. Padmanath and S. Prelovsek, Signature of a doubly charm tetraquark pole in DD^* scattering on the lattice, *Phys. Rev. Lett.* **129**, 032002 (2022).
- [15] E. J. Eichten and C. Quigg, Heavy-quark symmetry implies stable heavy tetraquark mesons $Q_i Q_j \bar{q}_k \bar{q}_l$, *Phys. Rev. Lett.* **119**, 202002 (2017).
- [16] E. Braaten, L.-P. He, and A. Mohapatra, Masses of doubly heavy tetraquarks with error bars, *Phys. Rev. D* **103**, 016001 (2021).
- [17] D. Ebert, R. N. Faustov, V. O. Galkin, and W. Lucha, Masses of tetraquarks with two heavy quarks in the relativistic quark model, *Phys. Rev. D* **76**, 114015 (2007).
- [18] H. J. Lipkin, A model independent approach to multi-quark bound states, *Phys. Lett. B* **172**, 242 (1986).
- [19] S. Zouzou, B. Silvestre-Brac, C. Gignoux, and J. M. Richard, Four quark bound states, *Z. Phys. C* **30**, 457 (1986).
- [20] B. Silvestre-Brac and C. Semay, Systematics of $L = 0$ q-2 anti-q-2 systems, *Z. Phys. C* **57**, 273 (1993).
- [21] C. Semay and B. Silvestre-Brac, Diquonia and potential models, *Z. Phys. C* **61**, 271 (1994).
- [22] S. H. Lee and S. Yasui, Stable multiquark states with heavy quarks in a diquark model, *Eur. Phys. J. C* **64**, 283 (2009).
- [23] M. Karliner and J. L. Rosner, Discovery of doubly-charmed Ξ_{cc} baryon implies a stable $(bb\bar{u}\bar{d})$ tetraquark, *Phys. Rev. Lett.* **119**, 202001 (2017).
- [24] T. F. Caramés, J. Vijande, and A. Valcarce, Exotic $bc\bar{q}\bar{q}$ four-quark states, *Phys. Rev. D* **99**, 014006 (2019).
- [25] W. Park, S. Noh, and S. H. Lee, Masses of the doubly heavy tetraquarks in a constituent quark model, *Nucl. Phys. A* **983**, 1 (2019).
- [26] Q.-F. Lü, D.-Y. Chen, and Y.-B. Dong, Masses of doubly heavy tetraquarks T_{QQ} in a relativized quark model, *Phys. Rev. D* **102**, 034012 (2020).
- [27] T. Guo, J. Li, J. Zhao, and L. He, Mass spectra of doubly heavy tetraquarks in an improved chromomagnetic interaction model, *Phys. Rev. D* **105**, 014021 (2022).
- [28] J.-M. Richard, A. Valcarce, and J. Vijande, Doubly-heavy tetraquark bound states and resonances, *Nucl. Part. Phys. Proc.* **324–329**, 64 (2023).
- [29] Y. Song and D. Jia, Mass spectra of doubly heavy tetraquarks in diquark—antidiquark picture, *Commun. Theor. Phys.* **75**, 055201 (2023).
- [30] S. Sakai, L. Roca, and E. Oset, Charm-beauty meson bound states from $B(B^*)D(D^*)$ and $B(B^*)\bar{D}(\bar{D}^*)$ interaction, *Phys. Rev. D* **96**, 054023 (2017).
- [31] C. Deng, H. Chen, and J. Ping, Systematical investigation on the stability of doubly heavy tetraquark states, *Eur. Phys. J. A* **56**, 9 (2020).
- [32] G. Yang, J. Ping, and J. Segovia, Double-heavy tetraquarks, *Phys. Rev. D* **101**, 014001 (2020).
- [33] Y. Tan, W. Lu, and J. Ping, Systematics of $QQ\bar{q}\bar{q}$ in a chiral constituent quark model, *Eur. Phys. J. Plus* **135**, 716 (2020).
- [34] W. Chen, T. G. Steele, and S.-L. Zhu, Exotic open-flavor $bc\bar{q}\bar{q}$, $bc\bar{s}\bar{s}$ and $qc\bar{q}\bar{b}$, $sc\bar{s}\bar{b}$ tetraquark states, *Phys. Rev. D* **89**, 054037 (2014).
- [35] S. S. Agaev, K. Azizi, B. Barsbay, and H. Sundu, Weak decays of the axial-vector tetraquark $T_{bb;\bar{u}\bar{d}}^-$, *Phys. Rev. D* **99**, 033002 (2019).
- [36] S. S. Agaev, K. Azizi, B. Barsbay, and H. Sundu, Heavy exotic scalar meson $T_{bb;\bar{u}\bar{s}}^-$, *Phys. Rev. D* **101**, 094026 (2020).
- [37] S. S. Agaev, K. Azizi, B. Barsbay, and H. Sundu, A family of double-beauty tetraquarks: Axial-vector state $T_{bb;\bar{u}\bar{s}}^-$, *Chin. Phys. C* **45**, 013105 (2021).
- [38] Q.-N. Wang and W. Chen, Fully open-flavor tetraquark states $bc\bar{q}\bar{s}$ and $sc\bar{q}\bar{b}$ with $J^P = 0^+, 1^+$, *Eur. Phys. J. C* **80**, 389 (2020).
- [39] H. Mutuk, Masses and magnetic moments of doubly heavy tetraquarks via diffusion Monte Carlo method, *Eur. Phys. J. C* **84**, 395 (2024).
- [40] A. Francis, R. J. Hudspith, R. Lewis, and K. Maltman, Evidence for charm-bottom tetraquarks and the mass dependence of heavy-light tetraquark states from lattice QCD, *Phys. Rev. D* **99**, 054505 (2019).
- [41] R. J. Hudspith, B. Colquhoun, A. Francis, R. Lewis, and K. Maltman, A lattice investigation of exotic tetraquark channels, *Phys. Rev. D* **102**, 114506 (2020).
- [42] S. Meinel, M. Pflaumer, and M. Wagner, Search for b^-b^-us and b^-b^-ud tetraquark bound states using lattice QCD, *Phys. Rev. D* **106**, 034507 (2022).

- [43] M. Padmanath, A. Radhakrishnan, and N. Mathur, Bound isoscalar axial-vector $bc\bar{u}\bar{d}$ tetraquark T_{bc} from lattice QCD using two-meson and diquark-antidiquark variational basis, *Phys. Rev. Lett.* **132**, 201902 (2024).
- [44] C. Alexandrou, J. Finkenrath, T. Leontiou, S. Meinel, M. Pflaumer, and M. Wagner, Shallow bound states and hints for broad resonances with quark content b^-c^-ud in $B-D^-$ and B^*-D^- scattering from lattice QCD, *Phys. Rev. Lett.* **132**, 151902 (2024).
- [45] P. Junnarkar and N. Mathur, Deuteronlike heavy dibaryons from lattice quantum chromodynamics, *Phys. Rev. Lett.* **123**, 162003 (2019).
- [46] S. Basak, S. Datta, N. Mathur, A. T. Lytle, P. Majumdar, and M. Padmanath (ILGTI Collaboration), Hadron spectra and Δ_{mix} from overlap quarks on a HISQ sea, *Proc. Sci., LATTICE2014* (2015) 083 [arXiv:1412.7248].
- [47] M. Padmanath and N. Mathur, Quantum numbers of recently discovered Ω_c^0 baryons from lattice QCD, *Phys. Rev. Lett.* **119**, 042001 (2017).
- [48] S. Basak, S. Datta, M. Padmanath, P. Majumdar, and N. Mathur, Charm and strange hadron spectra from overlap fermions on HISQ gauge configurations, *Proc. Sci., LATTICE2012* (2012) 141 [arXiv:1211.6277].
- [49] S. Basak, S. Datta, A. T. Lytle, M. Padmanath, P. Majumdar, and N. Mathur, Hadron spectra from overlap fermions on HISQ gauge configurations, *Proc. Sci., LATTICE2013* (2014) 243 [arXiv:1312.3050].
- [50] N. Mathur, M. Padmanath, and R. Lewis, Charmed-bottom mesons from lattice QCD, *Proc. Sci., LATTICE2016* (2016) 100 [arXiv:1611.04085].
- [51] N. Mathur, M. Padmanath, and S. Mondal, Precise predictions of charmed-bottom hadrons from lattice QCD, *Phys. Rev. Lett.* **121**, 202002 (2018).
- [52] N. Mathur and M. Padmanath, Lattice QCD study of doubly charmed strange baryons, *Phys. Rev. D* **99**, 031501(R) (2019).
- [53] P. M. Junnarkar and N. Mathur, Study of three-flavored heavy dibaryons using lattice QCD, *Phys. Rev. D* **106**, 054511 (2022).
- [54] N. Mathur, M. Padmanath, and D. Chakraborty, Strongly bound dibaryon with maximal beauty flavor from lattice QCD, *Phys. Rev. Lett.* **130**, 111901 (2023).
- [55] A. Bazavov *et al.* (MILC Collaboration), Lattice QCD ensembles with four flavors of highly improved staggered quarks, *Phys. Rev. D* **87**, 054505 (2013).
- [56] E. Follana, Q. Mason, C. Davies, K. Hornbostel, G. P. Lepage, J. Shigemitsu, H. Trotter, and K. Wong (HPQCD, UKQCD Collaborations), Highly improved staggered quarks on the lattice, with applications to charm physics, *Phys. Rev. D* **75**, 054502 (2007).
- [57] Y. Chen, S. J. Dong, T. Draper, I. Horvath, F. X. Lee, K. F. Liu, N. Mathur, and J. B. Zhang, Chiral logarithms in quenched QCD, *Phys. Rev. D* **70**, 034502 (2004).
- [58] A. Li *et al.* (xQCD Collaboration), Overlap valence on 2 + 1 flavor domain wall fermion configurations with deflation and low-mode substitution, *Phys. Rev. D* **82**, 114501 (2010).
- [59] A. X. El-Khadra, A. S. Kronfeld, and P. B. Mackenzie, Massive fermions in lattice gauge theory, *Phys. Rev. D* **55**, 3933 (1997).
- [60] B. Chakraborty, C. T. H. Davies, B. Galloway, P. Knecht, J. Koponen, G. C. Donald, R. J. Dowdall, G. P. Lepage, and C. McNeile, High-precision quark masses and QCD coupling from $n_f = 4$ lattice QCD, *Phys. Rev. D* **91**, 054508 (2015).
- [61] G. P. Lepage, L. Magnea, C. Nakhleh, U. Magnea, and K. Hornbostel, Improved nonrelativistic QCD for heavy-quark physics, *Phys. Rev. D* **46**, 4052 (1992).
- [62] A. Czarnecki, B. Leng, and M. B. Voloshin, Stability of tetrons, *Phys. Lett. B* **778**, 233 (2018).
- [63] R. J. Hudspith and D. Mohler, Exotic tetraquark states with two \bar{b} quarks and $J^P = 0^+$ and 1^+ B_s states in a non-perturbatively tuned lattice NRQCD setup, *Phys. Rev. D* **107**, 114510 (2023).
- [64] L. Leskovec, S. Meinel, M. Pflaumer, and M. Wagner, Lattice QCD investigation of a doubly-bottom $\bar{b}\bar{b}ud$ tetraquark with quantum numbers $i(J^P) = 0(1^+)$, *Phys. Rev. D* **100**, 014503 (2019).
- [65] P. Junnarkar, N. Mathur, and M. Padmanath, Study of doubly heavy tetraquarks in lattice QCD, *Phys. Rev. D* **99**, 034507 (2019).
- [66] P. Bicudo, M. Cardoso, A. Peters, M. Pflaumer, and M. Wagner, $ud\bar{b}\bar{b}$ tetraquark resonances with lattice QCD potentials and the Born-Oppenheimer approximation, *Phys. Rev. D* **96**, 054510 (2017).
- [67] A. Francis, R. J. Hudspith, R. Lewis, and K. Maltman, Lattice prediction for deeply bound doubly heavy tetraquarks, *Phys. Rev. Lett.* **118**, 142001 (2017).
- [68] P. Bicudo, K. Cichy, A. Peters, and M. Wagner, bb interactions with static bottom quarks from lattice QCD, *Phys. Rev. D* **93**, 034501 (2016).
- [69] C. Michael, Adjoint sources in lattice gauge theory, *Nucl. Phys.* **B259**, 58 (1985).
- [70] M. Luscher, Two particle states on a torus and their relation to the scattering matrix, *Nucl. Phys.* **B354**, 531 (1991).
- [71] M.-L. Du, A. Filin, V. Baru, X.-K. Dong, E. Epelbaum, F.-K. Guo, C. Hanhart, A. Nefediev, J. Nieves, and Q. Wang, Role of left-hand cut contributions on pole extractions from lattice data: Case study for $T_{cc}(3875)^+$, *Phys. Rev. Lett.* **131**, 131903 (2023).
- [72] A. B. a. Raposo and M. T. Hansen, Finite-volume scattering on the left-hand cut, arXiv:2311.18793.
- [73] L. Meng, V. Baru, E. Epelbaum, A. A. Filin, and A. M. Gasparyan, Solving the left-hand cut problem in lattice QCD: $T_{cc}(3875)^+$ from finite volume energy levels, *Phys. Rev. D* **109**, L071506 (2024).
- [74] M. T. Hansen, F. Romero-López, and S. R. Sharpe, Incorporating $DD\pi$ effects and left-hand cuts in lattice QCD studies of the $T_{cc}(3875)^+$, *J. High Energy Phys.* **06** (2024) 051.
- [75] S. Prelovsek, S. Collins, D. Mohler, M. Padmanath, and S. Piemonte, Charmonium-like resonances with $J^{PC} = 0^{++}$, 2^{++} in coupled $D\bar{D}$, $D_s\bar{D}_s$ scattering on the lattice, *J. High Energy Phys.* **06** (2021) 035.
- [76] M. Neubert, Heavy quark symmetry, *Phys. Rep.* **245**, 259 (1994).

- [77] T. Aoki, S. Aoki, and T. Inoue, Lattice study on a tetra-quark state T_{bb} in the HAL QCD method, *Phys. Rev. D* **108**, 054502 (2023).
- [78] C. Alexandrou, J. Finkenrath, T. Leontiou, S. Meinel, M. Pflaumer, and M. Wagner, $\bar{b}\bar{b}ud$ and $\bar{b}\bar{b}us$ tetraquarks from lattice QCD using symmetric correlation matrices with both local and scattering interpolating operators, [arXiv:2404.03588](https://arxiv.org/abs/2404.03588).
- [79] C. Morningstar, J. Bulava, B. Singha, R. Brett, J. Fallica, A. Hanlon, and B. Hörz, Estimating the two-particle K -matrix for multiple partial waves and decay channels from finite-volume energies, *Nucl. Phys.* **B924**, 477 (2017).